Tuning of Fluorescence in Films and Nanoparticles of Oligophenylenevinylenes

Dieter Oelkrug,*,†,‡ Alfred Tompert,† Johannes Gierschner,† Hans-Joachim Egelhaaf,† Michael Hanack,*,§,⊥ Michael Hohloch,§ and Elke Steinhuber§

Institute of Physical Chemistry and Institute of Organic Chemistry, University of Tübingen, Auf der Morgenstelle 8, D-72076 Tübingen, Germany

Received: October 2, 1997; In Final Form: December 21, 1997

Oligophenylenevinylenes (OPV) with a series of distance-controlling, electron-donating, and/or electron-withdrawing substituents are deposited from vapor phase and solution as ultrathin films or nanoparticles with diameters of 20−200 nm. In some cases the systems are doped at levels of 10^{-5}−10^{-3} with energy accepting OPV's of longer chainlengths. Absorption and fluorescence spectra, steady-state and time-resolved anisotropies, and radiative and nonradiative deactivation rates of these systems are investigated and compared to the corresponding properties in dilute solutions. Fluorescence yields of the parent oligomers and their alkyl or oxyalkyl derivatives are high in solution with an "infinite chain" limit of $\Phi_F \approx 0.5$ and an upper radiative rate constant limit of $k_r^\infty = (1 \pm 0.3) \times 10^9\ s^{-1}$. Yields and k_r decrease strongly in films and nanoparticles because of H-aggregate formation. However, doping with fluorescent acceptors can increase the yields up to $\Phi_F \rightarrow 0.7$. Introduction of electron-withdrawing -CN and $-SO_2CF_3$ substituents reduces Φ_F in low viscous dilute solutions almost to zero. High viscosities and condensation to solid phases will raise the yields up to $\Phi_F \rightarrow 0.6$ because of suppression of nonradiative torsional deactivation and formation of J-aggregates with high k_r.

Introduction

Polyphenylenevinylenes (PPV) are widely investigated as candidates for applications in electroluminescence (EL) devices. Basic requirements for bright luminescence are high efficiencies of excited-state formation and of consecutive luminescence emission in the visible spectral range. The spectral position is determined mainly by the effective π-conjugation length in the excited state and by nonresonant or resonant coupling to surrounding electronic oscillators. The efficiency of luminescence depends on competing nonradiative processes by intramolecular and intermolecular vibronic interactions, and on excited-state diffusion to emissive or nonemissive traps. Thus the most important parameters which have to be optimized with respect to high luminescence efficiency are (i) geometrical structure and electronic conjugation of the emitting centers, (ii) nuclear dynamics, (iii) intermolecular orientation, (iv) chemical purity, and (v) specific doping.

Optical absorption and photoluminescence (PL) spectra of the parent oligophenylenevinylenes *n*PV up to $n = 6$ (with n representing the number of vinylene groups) and their *tert*-butyl-substituted derivates BnPV have been extensively studied in solution, solid powders, nanoparticles, and thin films.[1−4,5−8] Also the influences of substituents, especially of long alkyl or oxyalkyl chains and electron-withdrawing (-CN or $-SO_2CF_3$) groups, on EL and PL were analyzed.[9−13] In general the PL yields (Φ_F) are high in dilute solution ($\Phi_F > 0.5$) but low in the solid state. For unsubstituted PPV films, $\Phi_F = 0.04$−0.05 has been reported.[14] Freshly deposited amorphous 2PV films (compound **2** of Figure 1) are practically nonfluorescent, but fluorescence increases within hours to $\Phi_F = 0.1$−0.2 by transformation into nanocrystals.[15] Preparations of 2PV nanoparticles in liquid suspension yield $\Phi_F = 0.08$.[8] On the other hand, tailored substituents may increase the yields of polymer films to $\Phi_F = 0.35$[16] or even to $\Phi_F \approx 0.6$.[17] A similar high value was reported by us[12] for microcrystalline dicyano-dihexyl-2PV (compound **5a** of Figure 1). Obviously, nonradiative deactivation processes are strongly induced by intermolecular interactions, especially if the carbon backbones are able to form tight coplanar arrangements with strong intermolecular π-overlap.

Crystal and gas-phase structures are known only for stilbene (= 1PV). The planes of the two phenyl rings form an angle of $\vartheta = 7$−$15°$. A similar small deviation from planarity is found for crystalline tris(dioxypropyl)-2PV.[18] In dioxyoctyl-4PV, the torsional angle between outer and central phenyl ring is already $\vartheta = 30°$.[19] Additional cyano substituents in the vinylene moiety reduce torsion to $\vartheta = 15°$. However, introduction of cyano substituents into dialkyl-2PV **3** forming **5a** causes the opposite effect of very high torsional angles $\vartheta = 49°$ between the central and outer phenyl planes, and $\vartheta' = 27°$ between the central phenyl plane and direction of the vinylene group.[20] An even higher ϑ' is found in **5b** (Figure 2).[20]

This paper presents, in extension of earlier contributions,[2,3,8,12] a systematic investigation of the electronic and geometrical effects of substituents upon the positions of fluorescence bands, fluorescence quantum yields, and decay curves of oligomeric PPV homologues. Especially, the transition from dilute fluid solution to confined environments and the solid state is elucidated. Distance keeping and bipolar substituents are used in order to reduce intermolecular interactions in the solid state and to change the preferential side-by-side arrangement into a head-to-tail arrangement. Further, we describe solid-state doping experiments of short *n*PV's with dopants of longer

† Institute of Physical Chemistry.
‡ E-mail: dieter.oelkrug@uni-tuebingen.de.
§ Institute of Organic Chemistry.
⊥ E-mail: hanack@uni-tuebingen.de.

S1089-5647(97)03225-2 CCC: $15.00
Published on Web 02/20/1998

conjugation lengths which cause efficient excitation energy transfer and considerable enhancement of the fluorescence quantum yields.

Experimental Section

Materials. Starting from 1,4-distyrylbenzene (2PV, compound **2** of Figure 1) with $n = 2$ phenylenevinylene repetition units, the central phenylene ring is substituted with distance-keeping hexyl chains or electron-donating as well as distance-keeping oxyhexyl chains. In addition, the vinylene moieties are substituted at the peripheral or central positions with electron-accepting cyano (-CN) or triflyl ($-SO_2CF_3$) groups. Figures 1, 2, and 7 present the structural formulas of the corresponding compounds **3**−**8**. Their preparation is described elsewhere.[13] In addition, compound **1** with no terminal phenyl groups was synthesized via aldol condensation of 2,5-di-*n*-hexylterephthalaldehyde and acetonitrile with KOH as a base. Nanoparticles (diameters 20−200 nm) were precipitated from methanol/H_2O mixtures and measured in suspension. Doping experiments were carried out with 2PV as host and, as guests, methanol-soluble longer OPV's with four *tert*-butyl groups in the 3,3′,5,5′-positions of the terminal phenyl rings (= BnPV, formula at Figure 9) and $n = 3-6$ phenylenevinylene repetition units. The BnPV series was prepared by Müllen and coworkers.[21] Doped nanoparticles were precipitated from methanolic solutions containing 2PV and the dopant in molar ratios of $10^{-5}-10^{-3}$. Solid films were deposited onto fused silica from HV.

Fluorescence and Absorption Measurements. Fluorescence spectra were recorded on a Spex-Fluorolog 222, and absorption spectra on a Perkin-Elmer Lambda-2 UV/vis spectrometer. Fluorescence quantum yields of films were obtained according to the evaluation method described earlier.[22] Fluorescence yields of microcrystals were measured on thick powder layers with approximately total absorption against isopropylene-bridged Michler's ketone on silica gel as reference with $\Phi_F = 0.9$.[23] Fluorescence decay curves were measured on a Spex Fluorolog equipped with a nanosecond flashlamp, using the time-correlated single photon counting technique. Particle sizes of nanoparticles were determined by dynamic light-scattering measurements.

Results and Discussion

Absorption and Fluorescence Spectra in Solution. Figure 1 presents spectra of dicyanodivinylbenzene **1** and a series of 2PV derivates **2**−**6** ordered according to decreasing transition energies for emission. The fluorescence spectra are clearly vibrationally structured, but not the absorption spectra, indicating a better planarized carbon skeleton in the emitting state than in the electronic ground state. The spectra are comparable to biphenyl, where the phenyl rings are twisted against each other by $\vartheta = 50°$ in the ground state but form a planar molecule with $\vartheta \approx 0°$ in the first excited singlet or triplet state.[24,25] Unlike Figure 1, the examples of Figure 2 show unstructured fluorescence spectra, even upon cooling to 77 K. The cyano groups of these compounds are in close vicinity to the hexyl groups, preventing excited-state planarization by steric hindrance.

Starting from **2**, the transition energies of fluorescence decrease with the extension of the electronic wave functions in direction of **3** (weak electron-donating contribution of alkyl groups), **4** (medium donating contribution of oxyalkyl groups), **5a** (combination of alkyl with strongly accepting cyano groups), and **6** (combination of oxyalkyl with cyano groups). Substituents which prevent planarization will reduce the effective

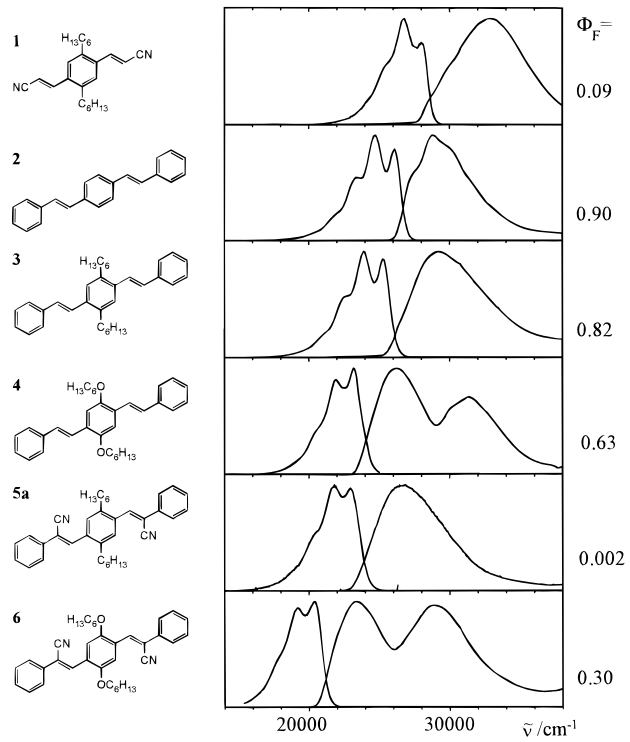

Figure 1. Fluorescence and absorption spectra of dicyanodivinylbenzene **1** and a series of 2PV derivatives **2**−**6** in *n*-hexane (**1**−**4**, **6**) or polyethylene (**5a**). Fluorescence quantum yields Φ_F in CH_2Cl_2 solution (**1**−**6**).

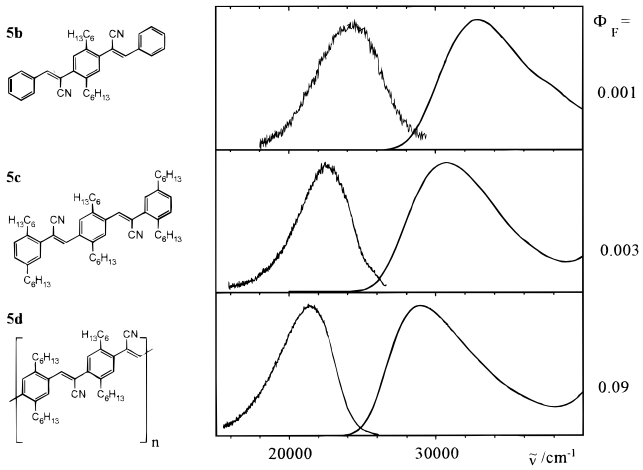

Figure 2. Fluorescence and absorption spectra and fluorescence quantum yields of 2PV derivatives **5b**−**d**, dissolved in CH_2Cl_2.

π-conjugation length in the excited state and create blue-shifted fluorescence spectra. This can be seen by comparing **5a** to **5b** or **5c**, where steric hindrance prevents planarization of the vinylene groups with the central ring (**5b**) or the peripheral rings (**5c**). Even polymerization to **5d** causes no significant additional redshift, so that the excited-state conjugation length of this nonplanar polymer is not much longer than in the dimeric subunit.

Fluorescence Quantum Yields in Solution. In all common solvents, the parent hydrocarbon **2** is highly fluorescent with a quantum yield Φ_F close to unity. Introduction of alkyl or oxyalkyl substituents reduces Φ_F to some extent, but fluorescence remains the dominant deactivation channel even for very long oligophenylenevinylenes. The oligomeric series with oxyalkyl and *tert*-butyl substituents allows extrapolation of the quantum yields to "infinite" chainlength resulting in $\Phi_F^{\infty} \rightarrow$

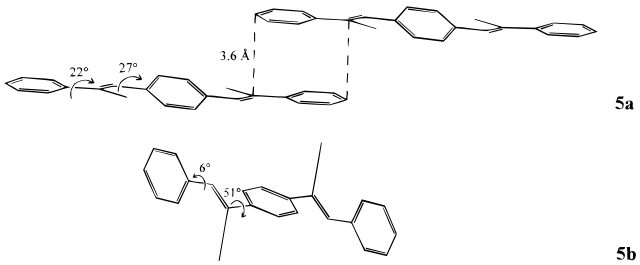

Figure 3. Geometrical arrangements of the carbon backbones of **5a** and **5b** in the crystalline state.[20]

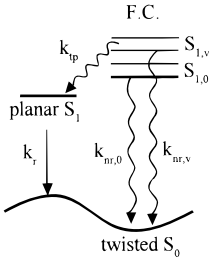

Figure 4. Schematic deactivation scheme of **5a**.

TABLE 1: Fluorescence Quantum Yields and Decay Times of 5a

matrix	$\Phi_F \approx k_{tp}/(k_{nr} + k_{tp})$	$\tau_F \approx k_r^{-1}$/ns
CH_2Cl_2, liq	0.002	
paraffin, liq	0.07	0.9
polyethylene, sol.	~0.2	1.3
EPA glass, $T = 77$ K	~0.5−0.8	1.5
alumina, microporous	~0.3	1.3
silica gel, microporous	~0.03	0.7
microcrystals	~0.5	1.05

0.4 and $\Phi_F^{\infty} \rightarrow 0.7$, respectively.[8,12] The small but systematic reduction of Φ_F with chainlength can be explained by the interplay of radiative and nonradiative rate constants. The former follows the n^{-1} relation, $k_r = k_r^{\infty} - a \cdot n^{-1}$, and saturates at $k_r^{\infty} = (1 \pm 0.3) \times 10^9$ s^{-1}. The latter increases with the density of torsional phonon states, i.e., approximately linearly with n. In total, the ratio of nonradiative to radiative processes increases with chainlength.

Introduction of cyano groups in the vinylene moieties considerably reduces Φ_F in all examples of Figures 1 and 2. The low yields are mainly a consequence of nonplanarity which enables torsional induced nonradiative deactivation by avoiding the planar quinoidal mesomeric structure in the S_1 state. Figure 3 shows the geometrical arrangements of the carbon backbones of **5a** and **5b** in the crystalline state.[20] It is obvious that these molecules are far away from planarity in the electronic ground state. On the other hand, the positions of the cyano groups in **5a** do not prevent planarization of the central molecular part in S_1. Thus, **5a** will emit if the rate k_{tp} of planarization is comparable to the torsional induced nonradiative deactivation rate k_{nr} of the initially excited Franck−Condon (F.C.) state. Table 1 lists fluorescence quantum yields and decay times of **5a** in solvents of different viscosities, confined environments, and crystalline state. The yields cover more than two orders of magnitude, but the decay times only a factor of 2. The deactivation scheme of Figure 4 presents a possible explanation for these results.

Highly viscous media or confined environments of micropores generate a potential barrier against torsional nonradiative deactivation in the F.C. state and facilitate planarization. The formation efficiency of the planar S_1 state is approximately equal to Φ_F since, in analogy with the other planar *n*PV's, nonradiative

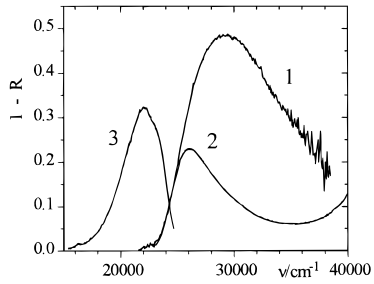

Figure 5. (1) Diffuse reflectance absorption spectrum ($1 - R_{diff}$) of **5a** physisorbed in microporous silica gel ($c = 0.2$ mg/g), (2) fluorescence excitation spectrum, (3) fluorescence emission spectrum of the same sample.

deactivation from the planar S_1 state is low against k_r. With the realistic additional assumption of $k_r \ll k_{tp}$, the fluorescence decay time will then be $\tau_F = k_r^{-1}$. Thus Φ_F and τ_F are not correlated to each other and can vary in a quite different way with the environment. The complex dynamics in the F.C. state can also be taken from the fluorescence excitation maxima which show a tendency to redshift against the absorption maxima. In paraffin, the shift amounts to $\Delta\lambda = 364 - 355 = 9$ nm, from which we conclude that torsional depopulation $k_{nr,v}$ of the vibrationally excited F.C. state is faster than $k_{nr,0}$ and faster than thermal equilibration. This effect is even more pronounced in the micropores of silica gel (Figure 5). Only the low energetic wing of the excitation spectrum follows the absorption spectrum. Then the curve bends, indicating a strong reduction in Φ_F upon high energetic excitation. Finally, the positions of the excitation maxima of casted **5a** films vary extremely with film thickness between $\lambda = 355$ and 388 nm, whereas the fluorescence maxima are stable at $\lambda = 469 \pm 1$ nm.

Absorption and Fluorescence Spectra in Films and Nanoparticles. Condensation of *n*PV's to solid phases will affect their photophysical properties mainly by intermolecular coupling of electronic transition dipole moments; reduction of torsional induced nonradiative deactivation processes; and migration of excitation energy to distortions, impurity traps, or deliberately added dopants.

Intermolecular coupling is successfully described with the molecular exciton model: parallel alignment of the transition dipoles μ_e shifts absorption to the blue and reduces the fluorescence rate k_r (H-aggregate); head-to-tail alignment shifts absorption to the red and enhances fluorescence (J-aggregate). Since μ_e of the first singlet transition is oriented parallel to the long molecular axis and since dipole−dipole interaction is proportional to [distance]$^{-3}$, J-aggregation will induce much smaller spectral changes than H-aggregation, especially in the unsubstituted *n*PV's. Figure 6 compares spectra of 2PV in solution, nanoparticles, spincasted film (which, in fact, is formed from nanocrystalline islands), and polycrystalline powder. The main absorption maximum is strongly blueshifted against solution which is typical for H-aggregates, whereas the weak peak A_1 is slightly redshifted. This peak is the origin of the highest energetic fluorescence peak F_1. The main part of fluorescence might be a vibrational progression of F_1, but the shoulder T in the excitation spectra of thick layers could be the origin as well. The absorption coefficient of T is in the order of $x = 10^{-4}$ or less of the maximum absorption coefficient, so that T can be assigned to impurity traps or to small portions of lattice distortions forming J-aggregates with allowed fluorescence (J-aggregates are already formed if adjacent 2PV's overlap with two of three benzene rings). The latter interpretation is supported by the fact that a similar preband is also observed in

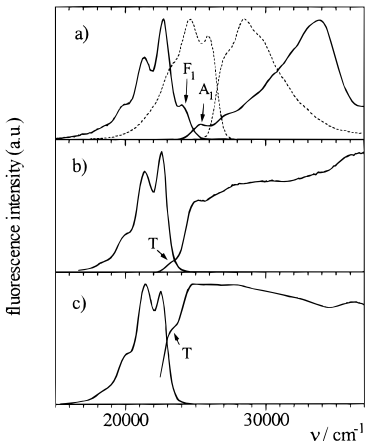

Figure 6. Fluorescence and fluorescence excitation spectra of 2PV: (a) nanoparticle suspension (solid lines) and single molecules dissolved in methanol (dashed lines); (b) spincasted film; (c) polycrystalline powder.

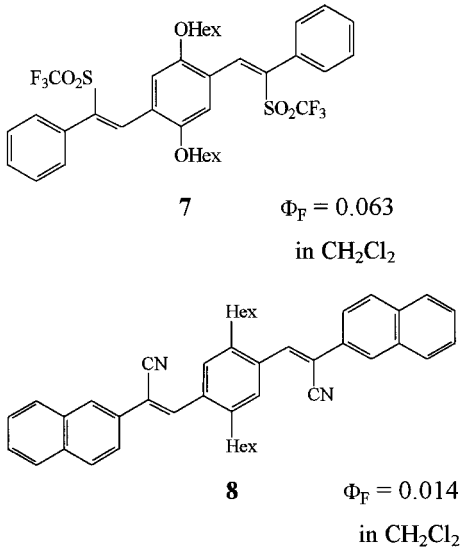

Figure 7. Structures of the triflyl-substituted 2PV (**7**) and the naphthyl-2PV (**8**).

3PV-aggregates. In addition, the main parts of 2PV and 3PV fluorescence are highly polarized, even better than F_1,[2] so that the emitting states must have the same orientation as the bulk lattice.

Introduction of bulky substituents in the peripherical rings reduces molecular exciton splitting because of larger intermolecular distances, but in principle H-aggregate formation is preserved. Introduction of alkyl or oxyalkyl chains in the central ring changes the intermolecular orientation in the direction of the cancelled dipole−dipole interaction or J-aggregation. Compound **7** (Figure 7), in which the cyano groups of **6** are replaced by bulky triflyl groups as electron acceptors, gives an example of very weak intermolecular interaction without large conformational changes upon excitation. The electronic origin of the solid material is identical with one of the molecules in solution (see Figure 8a), absorption and emission show mirror symmetry, and only the Stokes shift between absorption and fluorescence is reduced in the solid because of higher torsional barriers. The solid-state interaction in the less bulky compound **6** is enhanced against **7**, and correspondingly redshifted in fluorescence.[12]

As in solution,[12] **5a** shows some spectral peculiarities also in the solid. Absorption spectra of vapor-deposited or spincasted films are broad, and fluorescence is as strongly Stokes

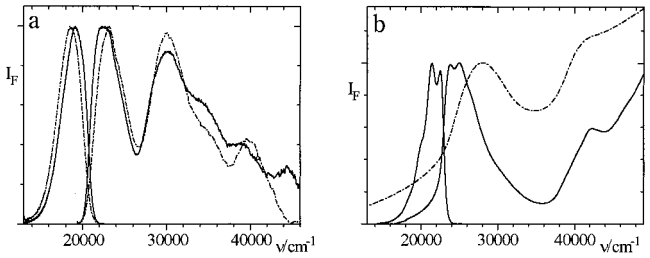

Figure 8. (a) Fluorescence emission and fluorescence excitation spectra of **7** in CH_2Cl_2 solution (dashed lines) and of microcrystals of the same compound (solid lines). (b) Absorption and fluorescence spectra of microcrystals of **5a** (solid lines) and absorption spectrum of a 30-nm vapor-deposited film of the same compound (dashed line).

TABLE 2: Fluorescence Quantum Yields of Nanoparticles (N), Films (F), and Polycrystalline Powders (P)

low $\Phi_F < 0.1$	medium $\Phi_F \approx 0.1-0.3$	high $\Phi_F \approx 0.5$
1, **2** (N)	**2** (P)	**5a** (P)
5b ($\Phi_F \approx 10^{-2}$)	**3**, **4**, **5a** (F)	**7** (P)
5c, **5d**	**6**	**8** (P)

shifted as in solution. However, after crystallization, the Stokes shift is strongly reduced (see Figure 8b) and the system behaves like J-aggregates with an intense onset of absorption and high fluorescence yields.

Fluorescence Quantum Yields of Films and Nanoparticles. Table 2 classifies some solid *n*PV's according to low, medium, and high fluorescence yields (exact numbers are not given because of the uncertainties in absorptivity, spatial anisotropy of emission, and fluorescence reabsorption). Compounds with rigid carbon backbones and not too many flexible side chains are highly fluorescent in solution, but exactly these types of molecules tend to form H-aggregates with close intermolecular contact. Thus the radiative rates of the solids become low, and intermolecular energy transfer, which finally ends at quenching sites, becomes very efficient. In sum the fluorescence yields of these materials are substantially lowered against the individual molecules. Compounds **2** (= 2PV), 3PV, **3**, and **4** are good examples of this type of fluorophore (in oligothiophenes the effect is even more pronounced[22]). The opposite behavior is found in **5a**, **7**, and **8** (Figure 7). Because of torsional deactivation, these compounds are very weakly fluorescent in solution but strongly in films or crystals. Fluorescence supporting properties are solid-state potential barriers against torsion, sufficient free volume for excited-state planarization, and J-aggregate formation (see Figure 3). Finally, **5b**, **5c**, and **5d** are weakly fluorescent as well in solution as in the solid state. Obviously intramolecular twisting is so strong in these compounds (see Figure 3) that even condensation does not substantially suppress nonradiative torsional deactivation.

Fluorescence of Doped 2PV Nanoparticles. The close intermolecular contacts and parallel orientations of 2PV (= **2**) in nanoparticles makes this medium suitable for efficient excitation transfer to lower energetic fluorescence centers, e.g., *n*PV's with $n > 2$. Molar fractions $x > 10^{-5}$ of these dopants are already sufficient to change the spectral distribution of fluorescence and to increase Φ_F. Figure 9 shows fluorescence spectra of "pure" **2** and after doping with small amounts of B5PV. New fluorescence bands appear, typical for single B5PV molecules in a highly polarizable environment, and the fluorescence yield increases with the mole fraction by a factor of up to 6 to $\Phi_F \approx 0.6$. The excitation spectrum of B5PV fluorescence is identical with the absorption spectrum of **2**, proving efficient host−guest energy transfer (Figure 9). Similar results are obtained with other *n*PV's and a series of oligo-

TABLE 3: Luminescence Data of 2PV−Nanoparticles Doped with 3PV and B5PV (x = mole fraction of dopant): Fluorescence Quantum Yields Φ_F and Fluorescence Decay Components τ_i with Amplitudes in Parentheses

			decay components τ_i/ns (rel ampl)			
			host		dopant	
host/dopant	x	integral Φ_F	293 K	50 K	293 K	50 K
2PV/−	−	0.08	2.1 (0.76) 3.8 (0.24)	2.3 (0.61) 11.6 (0.39)	−	−
2PV/3PV	1.2×10^{-3}	0.48	−	−	0.8 (−1.00) 1.9 (0.71) 5.0 (0.38)	−
2PV/B5PV	7.3×10^{-4}	0.34	1.3 (0.42) 3.5 (0.58)	2.0 (0.17) 7.6 (0.83)	0.6 (−1.00) 4.2 (1.13)	0.5 (−1.00) 5.9 (1.13)

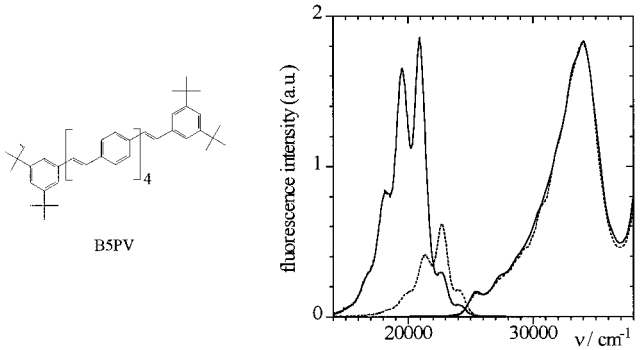

Figure 9. Fluorescence and fluorescence excitation spectra of 2PV-nanoparticle suspensions: (dashed lines) undoped, excitation spectrum scanned for fluorescence at $\tilde{\nu}_{em} = 22\,000$ cm^{-1}, (solid lines) doped with B5PV (mole fraction $x = 7.3 \times 10^{-4}$), $\tilde{\nu}_{em} = 17\,500$ cm^{-1}.

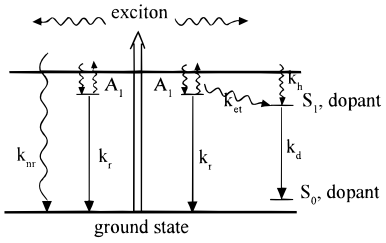

Figure 10. Electronic deactivation and energy transfer in doped *n*PV aggregates (schematic).

thiophenes. Details of this investigation will be given elsewhere. Upon cooling, the intensity of sensitized fluorescence first decreases, but then increases at temperatures below $T = 100$ K. The host fluorescence increases monotonically, and in total the intensity ratio guest/host is lower at $T = 50$ K than at room temperature.

Time-resolved fluorescence shows a rise component with $\tau = 0.5-0.8$ ns which is equal to the lifetime of directly excited B5PV in solution,[8] and a much longer, approximately exponential decay curve with a lifetime in the range of 3−5 ns. This range is valid for all concentrations of $x = 5 \times 10^{-5}-10^{-3}$ and also for all *n*PV and BnPV dopants with $n = 3-6$. The fluorescence decay of the host is nonexponential with decay components in the range of $\tau_i = 1-5$ ns, depending on x. At $T = 50$ K the long decay time component of undoped 2PV increases to $\tau = 9-11$ ns. With B5PV as dopant, the decay of the host is nonexponential and shortened to an average of $\tau = 5.7$ ns. For the guest, the decay time is approximately $\tau = 6$ ns (Table 3).

Although we are not able to present a consistent deactivation scheme at the present stage of investigation, Figure 10 may help to explain some of the experimental results. After excitation of the molecular exciton band, partly the vibrationally relaxed localized A_1 states are formed, and partly the energy dissipates nonradiatively with the rate constant k_{nr} at the electronically forbidden low-energy edge of the exciton band. The intrinsic radiative lifetime of A_1 is in the order of $\tau_0 = 30$ ns. At room temperature, most of the A_1 states deactivate nonradiatively via the exciton band by thermal activation and energy hopping. This type of dispersive transport results in nonexponential decay curves. In the presence of a dopant, its S_1 state can be populated after excitation either by Förster energy transfer via A_1 with a rate coefficient k_{et} or, at room temperature, also via the exciton band with an effective hopping constant k_h. At very low temperatures only the Förster pathway is open which reduces the probability of S_1 population. Since S_1 is populated and depopulated as intermediate of a consecutive reaction, its fluorescence intensity follows the biexponential relation

$$I_F(t) \sim (k_{et} + k_h - k_d)^{-1}[\exp(-k_d/t) - \exp(-(k_{et} + k_h)t)] \quad (1)$$

where k_d is the deactivation rate constant of the excited dopant. The rise component of eq 1 is determined by the faster of the two exponentials and the decay component by the slower one. In our systems always $k_d \gg k_{et} + k_h$ so that the fluorescence decay time of the dopant is given by $\tau_D = (k_{et} + k_h)^{-1}$.

Conclusions

Unsubstituted oligophenylenevinylenes show high fluorescence quantum yields in solution. In the solid state, fluorescence yields are low, accompanied by blue-shifted absorption and red-shifted fluorescence due to H-aggregation.

Electron-donating substituents at the phenyl rings cause spectral red-shifts without affecting fluorescence yields in solution. Addition of electron-accepting substituents at the vinylene moieties causes further red-shift and strong reduction of fluorescence yields. The low yields are mainly a consequence of nonplanarity caused by steric hindrance between the substituents which enables torsional induced nonradiative deactivation.

Highly viscous or rigid environments suppress torsional induced nonradiative deactivation and facilitate planarization of the molecules, thus strongly favoring fluorescence. However, in compounds with extreme intramolecular twisting, even condensation does not substantially increase fluorescence yields. In the solid state, bulky substituents reduce exciton splitting due to larger intermolecular distances. In some cases, alkyl or oxyalkyl groups at the central rings cause J-aggregation instead of H-aggregation. Doping *p*-distyrylbenzene **2** with oligomers of longer chain lengths causes efficient excitation transfer to these energy acceptors. Fluorescence quantum yields are strongly enhanced with increasing molar fractions of the dopant.

Acknowledgment. We thank K. Müllen (MPI für Polymerforschung, Mainz) for providing us with the BnPV series and U. Stalmach (Universität Mainz) for preparing 3PV. This work

was financially supported by the Deutsche Forschungsgemeinschaft.

References and Notes

(1) (a) Drefahl, G.; Kühnstedt, R.; Oswald, H.; Hörhold, H. H. *Makromol. Chem.* **1970**, *131*, 89; (b) Erckel, R.; Frühbeis, H. *Z. Naturforschung* **1982**, *37b*, 1472.

(2) Egelhaaf, H.-J.; Gierschner, J.; Oelkrug, D. *Synth. Met.* **1996**, *83*, 221.

(3) Gierschner, J.; Egelhaaf, H.-J.; Oelkrug, D. *Synth. Met.* **1997**, *84*, 529.

(4) Cornil, J.; Beljonne, D.; dos Santos, D. A.; Brédas, J. L. (a) *Synth. Met.* **1996**, *76*, 101; (b) *J. Phys. Chem.* **1995**, *99*, 5604.

(5) Tian, B.; Zerbi, G.; Schenk, R.; Müllen, K. *J. Chem. Phys.* **1991**, *95*, 3191.

(6) Woo, H. S.; Lhost, O.; Graham, S. C.; Bradley, D. D. C.; Friend, R. H.; Quattrocchi, C.; Brédas, J. L.; Schenk, R.; Müllen, K. *Synth. Met.* **1993**, *59*, 13.

(7) (a) Ohlemacher, A.; Schenk, R.; Weitzel, H. P.; Tyutylkov, N.; Tasseva, M.; Müllen, K. *Makromol. Chem.* **1992**, *193*, 81. (b) Karabunarliev, S.; Baumgarten, M.; Tyutylkov, N.; Müllen, K. *J. Phys. Chem.* **1994**, *98*, 11892.

(8) Oelkrug, D.; Egelhaaf, H.-J.; Gierschner, J.; Tompert, A. *Synth. Met.* **1996**, *76*, 249.

(9) (a) Greenham, N. C.; Moratti, S. C.; Bradley, D. D. C.; Friend, R. H.; Holmes, A. B. *Nature* **1993**, *365*, 628. (b) Baigent, D. R.; Hamer, P. J.; Friend, R. H.; Moratti, S. C.; Holmes, A. B. *Synth. Met.* **1995**, *71*, 2175.

(10) Staring, E. G. J; Demandt, R. C. J. E.; Braun, D.; Rikken, G. L. J.; Kessener, Y. A. R. R.; Venhuizen, A. H. J.; van Knippenberg, M. M. F.; Bouwmans, M. *Synth. Met.* **1995**, *71*, 2179.

(11) Döttinger, S. E.; Hohloch, M.; Hohnholz, D.; Segura, J. L.; Steinhuber, E.; Hanack, M. *Synth. Met.* **1997**, *84*, 267.

(12) Oelkrug, D.; Tompert, A.; Egelhaaf, H.-J.; Hanack, M.; Steinhuber, E.; Hohloch, M.; Meier, H.; Stalmach, U. *Synth. Met.* **1996**, *83*, 231.

(13) Döttinger, S. E.; Hohloch, M.; Segura, J. L.; Steinhuber, E.; Hanack, M.; Tompert, A.; Oelkrug, D. *Adv. Mater.* **1997**, *9*, 233.

(14) Köpping-Grem, G.; Leising, G.; Schimetta, M.; Stelzer, F.; Huber, A. *Synth. Met.* **1996**, *76*, 53.

(15) Egelhaaf, H.-J.; Brun, M.; Reich, S.; Oelkrug, D. *J. Mol. Struct.* **1992**, *267*, 297.

(16) Samuel, I. D. W.; Rumbles, G.; Collison, C. J.; Crystall, B.; Moratti, S. C.; Holmes, A. B. *Synth. Met.* **1996**, *76*, 15.

(17) Bradley, D. D. C. In Proc. Symp. M, E-MRS 1997 Spring Meeting, Strasbourg, submitted.

(18) (a) Stalmach, U. Ph.D. Thesis, Universität Mainz, 1996. (b) Stalmach, U.; Schollmeyer, D.; Meier, H. In preparation.

(19) Gill, R. E.; Hilberer, A.; van Hutten, P. F.; Berentschot, G.; Werts, M. P. L.; Meetsma, A.; Wittmann, J.-C.; Hadziioannou, G. *Synth. Met.* **1997**, *84*, 637.

(20) Hanack, M.; Hohloch, M.; Maichle-Mössmer, C. *Chem. Mater.*, in press.

(21) Schenk, R.; Gregorius, H.; Meerholz, K.; Heinze, J.; Müllen, K. *J. Am. Chem. Soc.* **1991**, *113*, 2634.

(22) Oelkrug, D.; Egelhaaf, H.-J.; Wilkinson, F.; Worrall, D. R. *J. Fluoresc.* **1995**, *6*, 165.

(23) Oelkrug, D. Fluorescence spectroscopy in turbid media and tissues. In *Topics in fluorescence spectroscopy*; Lakowicz, J. R., Ed.; Plenum Press: New York, 1994; Vol. 4, 223−254.

(24) Negri, F.; Zgierski, M. Z. *J. Chem. Phys.* **1992**, *97*, 7124.

(25) Im, H.-S.; Bernstein, E. R. *J. Chem. Phys.* **1988**, *88*, 7337.